Modeling of grating assisted standing wave microresonators for filter applications in integrated optics

Manfred Hammer*, Didit Yudistira, Remco Stoffer

MESA+ Research Institute, University of Twente, Enschede, The Netherlands

Abstract: A wide, multimode segment of a dielectric optical waveguide, enclosed by Bragg reflectors and evanescently coupled to adjacent port waveguides, can constitute the cavity in an integrated optical microresonator. It turns out that the device can be described adequately in terms of an approximate coupled mode theory model which involves only a few guided modes as basis fields. By reasoning along the coupled mode model, we motivate a simple design strategy for the resonator device. Rigorous two dimensional mode expansion simulations are applied to verify the predictions of the approximate model. The results exemplify the specific spectral response of the standing wave resonators. As refinements we discuss the single resonance of a device with nonsymmetrically detuned Bragg reflectors, and the cascading of two Fabry-Perot cavities, where the coupling across an intermediate shorter grating region establishes a power transfer characteristic that is suitable for an add-drop filter.

Keywords: integrated optics, numerical modeling, coupled mode theory, waveguide Bragg gratings, optical microresonators, rectangular microcavities

PACS codes: 42.82.–m 42.82.Et

1 Introduction

Optical microresonators are at present discussed as building blocks for large scale integrated optics [1, 2, 3, 4], typically for applications related to wavelength division multiplexing in optical telecommunications. Cross-connects, filters, or entire transceiver devices were proposed / realized, that rely on many, more or less uniform microresonators as basic elements. Traditionally [5] the focus is on resonators with circular disk- or ring shaped cavities [6, 7, 8, 9, 10, 11, 12, 13], although also elliptical [14, 15], rectangular [16, 17, 18], or other, more irregular shapes [19] have been considered.

One aims at compact devices, designed within material systems with high refractive index contrast, where frequently the application itself (switching, routing, modulation) [1, 20, 21] or imperfections or fluctuations in the technological realization [22, 23, 24] require a facility for post fabrication adjustment. In case the tuning is to be realized by electrooptical means, a major obstacle may be encountered in the form of the strong anisotropy of some of the most promising electrooptic materials [25, 4]. If for tuning purposes a piece of a highly anisotropic electrooptic crystal is present in the cavity ring, the permittivity that is sensed by the circulating wave changes with the angular propagation distance. Depending on the crystal orientation, the anisotropy may lead to a pronounced modulation, if not to leakage, of the optical waves, i.e. to a lossy cavity.

These problems can be avoided in standing wave resonators, where the light propagation is restricted basically to one axis. Integrated optical microresonators with square or rectangular cavities have attracted attention only quite recently [16, 17, 18, 26]. In their conventional form, where a rectangular segment of a dielectric waveguide serves as the cavity, also these concepts have a severe technological drawback: A quite high refractive index contrast is required for the total reflection effect at the cavity facets [27]; with the presently available materials a realization seems to be difficult.

A way out is found by replacing the waveguide facets by Bragg reflectors. This leads to a concept for a standing wave resonator in the form of a Fabry-Perot cavity that is laterally, evanescently coupled to two parallel port waveguides. Figure 1 sketches the structure that is to be discussed. While a parameterized time-domain coupled mode theory model is given in Ref. [16], so far apparently neither rigorous nor approximate simulations of these devices exist. This is what we would like to provide with this paper (preliminary results were already contained in Ref. [28]). In the next Section 2.1, we outline a simple, somewhat heuristic strategy how to select the many

*Department of Applied Mathematics, University of Twente   P.O. Box 217, 7500 AE Enschede, The Netherlands
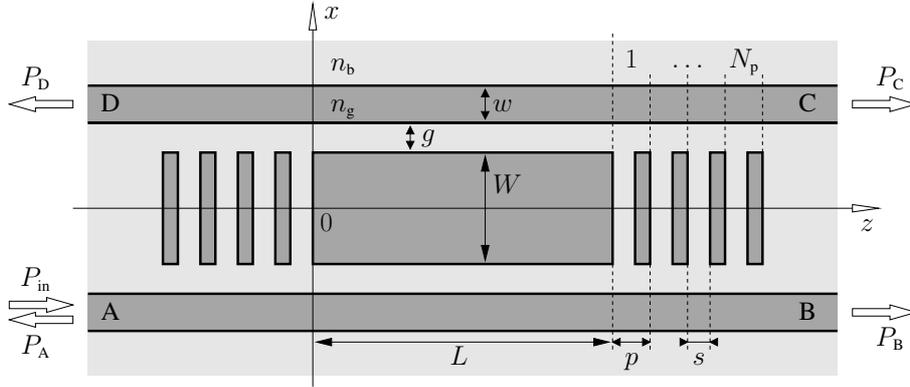*Phone: +31/53/489-3448*   *Fax: +31/53/489-4833*   *E-mail: m.hammer@math.utwente.nl*

Figure 1: Grating assisted rectangular resonator: Two parallel waveguide cores of width w are coupled by a cavity of width W and length L, separated by gaps g. Gratings with N_p periods of length p with a spacing s enclose the cavity. The guiding regions with refractive index n_g are embedded in a background medium with index n_b. Capital letters A to D denote the input and output ports.

parameters in the resonator specification. Section 3.1 summarizes the simulations of the resulting resonator device. In Sections 3.2, 3.3 the model is extended towards a resonator with nonidentical Bragg reflectors and towards an add-drop filter based on two cascaded cavities.

For the simulations we can on the one hand rely on rigorous mode expansion or bidirectional eigenmode propagation simulations [29, 30], specifically on the algorithms as described in Refs. [31, 17] and on the commercial tool [32]. On the other hand, we apply an ab-initio coupled mode theory model [18], briefly outlined in Section 2.2, that can be regarded as a direct implementation of the abstract design heuristics. This approach provides the best qualitative and also some quantitative insight in the device functionality.

Although the present concept requires the technological means to realize highly reflecting and low loss Bragg reflectors and may lead to relatively long devices, when compared to circular cavities, this type of resonator shows several quite advantageous features (apart from the restriction to basically one axis of propagation). Being formed by a straight waveguide segment, the cavity can be shortened or extended as necessary, without introducing additional losses as in the case of a ring or disk. While for circular cavities the adjustment of the proper strength of interaction with the port waveguides turns out to be a technological challenge (that led to concepts of vertical coupling [33] or "racetrack" shaped devices [8]), for the straight Fabry-Perot resonators the full length of the cavity is available for the coupling to the port waveguides; controlling the total coupling strength should be less critical.

2 Modeling

For purposes of qualitatively understanding the operation of the devices as introduced in Figure 1, it is helpful to initially resolve the resonator into parts. The central segment, extending from $z = 0$ to $z = L$, can be viewed as a three-core directional coupler that combines a wide multimode cavity waveguide and the two unimodal port waveguides. Two reflectors enclose the cavity, consisting of finite Bragg gratings that are etched into the wide cavity core.

It will turn out below (see Section 2.2) that a quantitative model on the basis of only one, forward and backward propagating guided mode of the central waveguide leads to a quite adequate description of the device. Two mechanisms are relevant to select that most relevant basis mode. On the one hand, with the port waveguides connected to the cavity in a regime of weak coupling, a phase matching condition involving the effective mode indices of the port waveguides and of the cavity mode has to be satisfied. On the other hand, lower modal reflectivities of the Bragg gratings suppress resonances that are related to modes other than the specific cavity mode. This motivates the somewhat heuristic reasoning in Section 2.1.

For simplicity, all considerations are restricted to two spatial dimensions and to TE polarization ("scalar" simulations). Nevertheless, one could regard the 2D permittivity profile as the result of the projection of a more realistic 3D structure in terms of effective indices. In the appendix we briefly comment on this viewpoint.

2.1 Design procedure

Given refractive indices n_g, n_b for the cores and the background, as a starting point of the resonator design we choose the width w of the port waveguides, such that these are single mode in a suitable wavelength region around the target wavelength $\lambda_0 = 1.55\,\mu$m; the values of Table 1 lead to an effective mode index $n_{\text{eff}} = 1.540$ at λ_0. According to the considerations above, only one guided mode of the cavity core is likely to be relevant for specific standing wave resonances. This field is to be excited in the cavity; hence, to satisfy the phase matching condition, we adjust W such that the cavity waveguide supports a guided mode that is degenerate with the port fields. Due to the purely harmonic shape of the profiles inside the core, modes with equal propagation constant at the same vacuum wavelength are found for a series of waveguides with increasing, equidistant widths. In the present case, W should be among the discrete values $(1.0 + m\,1.791)\,\mu$m, for integer m.

Pronounced resonances require a reflectivity close to unity for the relevant modes at the ends of the cavity [18]. The corresponding Bragg reflectors can be constructed on the basis of a model of tilted plane wave incidence on a multilayer stack with equivalent refractive index composition (cf. e.g. Ref. [34]). As indicated in Figure 2, we consider an incidence angle θ that corresponds to the angle of the relevant mode in the cavity, defined by $\cos\theta = n_{\text{eff}}/n_g$. The stack consists of $2\,N_p$ alternating, laterally infinite layers of thicknesses s (refractive index n_b) and $p - s$ (refractive index n_g) enclosed between half infinite media with refractive index n_g on the incidence side and n_b on the second side. Optimization of the configuration for the present mode angle of $15.69°$ at λ_0 leads to the grating parameters p and s as given in Table 1. The comparison with more rigorous simulations in Figure 3 confirms this — rather crude — approximation.
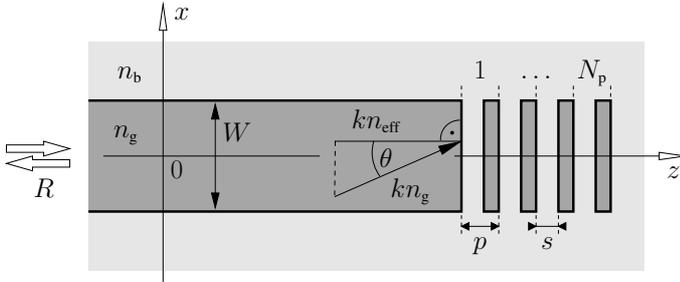

Figure 2: A single Bragg reflector, part of the resonator model.

To select a suitable cavity width W or mode order m, respectively, we computed single mode reflectivities for Bragg gratings according to the specification of Table 1 and Figure 1, for $N_p = 5$ and $W = (1.0 + m\,1.791)\,\mu$m, in each case for incidence of the m-th order mode. Levels of $0.17, 0.21, 0.23, 0.24, 0.25, 0.26$ were observed for $m = 0, 1, \ldots, 5$, with the last value already close to the limiting level of 0.28, the reflectivity of a plane wave, incident under an angle of $15.69°$ on a laterally unbounded equivalent multilayer stack as defined above. Apparently the larger the fraction of the mode profile is that actually encounters the corrugation of the Bragg reflector, the higher is the reflectivity. Therefore a width W corresponding to a higher order mode is preferred, (such that the phase matching condition is still sufficient to distinguish the cavity modes, the propagation constants of which become closer for large W). We set W to the value for order $m = 5$ for the present simulations.

Figure 3 shows that in this way indeed a suitable Bragg grating can be designed. Spectral reflectivity curves as predicted by three different types of simulations are compared. One observes a — quite surprising — agreement between the plane wave model and calculations by coupled mode theory (Section 2.2) and rigorous mode expansion (Section 3).

Given the complex valued amplitude reflection coefficient $r\,\exp \text{i}\varphi$ of the Bragg gratings, a resonance at λ_0 requires the total phase gain along one propagation cycle through the cavity to match an integer multiple of π. This amounts to a condition $L = (l\pi + \varphi)\lambda_0/(2\pi n_{\text{eff}})$ for the cavity length [18], with integer l. Neglecting the wavelength dependence of n_{eff} and assuming a long cavity $l\pi \gg \varphi$, one obtains $\Delta\lambda = \lambda_0/l = \lambda_0^2/(2Ln_{\text{eff}})$ for the spectral distance of two neighboring resonances. L, or l, respectively, is to be selected such that there is a chance for pronounced resonances in the window of high Bragg reflectivity around the design wavelength (l is about 159 in Figure 4).

Finally the gap width g is to be determined such that on the one hand there is a sufficient power transfer between the port waveguide and the cavity along the long unfolded light path in case of a resonance, while on the other
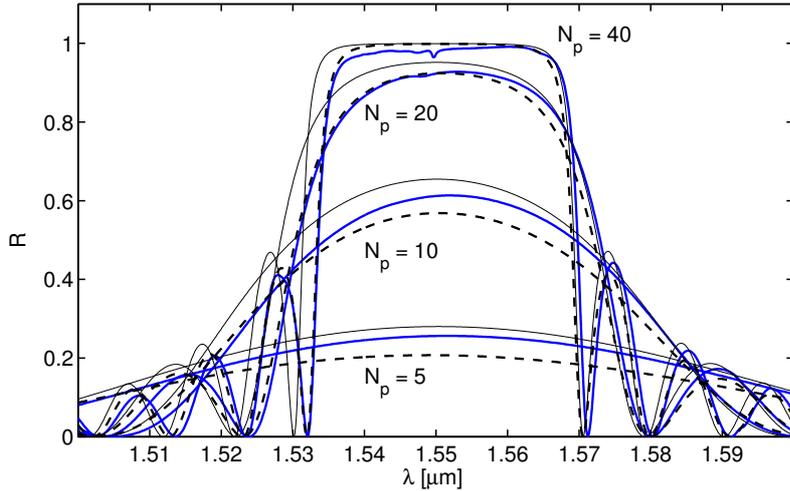
Figure 3: Power reflectivity R of Bragg-reflectors according to the specification of Figure 2 and Table 1, versus the vacuum wavelength, for different numbers of grating periods N_p. The guided 5-th order mode is launched in the wide cavity waveguide segment; the bold lines (continuous: rigorous mode expansion simulations, dashed: CMT results) show the relative power levels that are reflected into that specific mode. The thin curves indicate the plane wave reflectivity of an equivalent multilayer stack for wave incidence under the respective mode angle (15.69° at $\lambda = 1.55\,\mu m$).

hand the level of direct, nonresonant, unidirectional coupling (as in a conventional three-guide directional coupler, without a pronounced wavelength dependence over the range of practical importance) remains negligible. With this parameter being selected on the basis of numerical experiments, we arrived at the list of parameters of Table 1.

n_g	n_b	$w/\mu m$	$g/\mu m$	$W/\mu m$	$L/\mu m$	$p/\mu m$	$s/\mu m$	N_p	$\lambda/\mu m$
1.60	1.45	1.000	1.600	9.955	79.985	1.538	0.281	40	$\in [1.5, 1.6]$

Table 1: Geometrical and material parameters for the simulations of Figures 4, 5. Including two Bragg reflectors and the cavity, the overall length of the device is $203\,\mu m$.

2.2 Coupled mode theory

Taking the decomposition into two Bragg gratings and a central, z-homogeneous coupler region literally, one can describe the resonator devices by properly combining different variants of coupled mode theory (CMT) [29, 35]. The notion of one most relevant mode in the cavity core as introduced above allows these calculations to be kept simple and highly efficient.

For the simulations of the Bragg reflectors we consider a description of the isolated grating structures (Figure 2) in terms of contradirectional coupled mode theory, based on the forward- and backward traveling versions of the 5-th order guided mode supported by the cavity core. Using only one most relevant ("phase matched") contribution of a Fourier decomposition of the grating corrugation along z, the 2×2-system of coupled mode equations can be solved analytically. One obtains an approximation of the complex valued modal reflectivity of the Bragg gratings. Our implementation of that strategy follows the formulation given in Refs. [36, 37]. Results computed in this way are included in Figures 3, 6. Concerning the position of the bandgap and the form of the sidelobes, one observes a somehow unexpected agreement with the more rigorous results, given the quite substantial refractive index contrast in the present gratings. The CMT equations distribute the optical power among the two basis modes only. Losses to lateral radiation are not included, hence the top of the bandgap appears to be horizontal in the CMT description. In contrast to the plane wave model, the CMT takes the finite lateral extension W of the waveguide into account.

A CMT model for the central coupler segment can be based upon the three guided fields of the cavity (again only the 5-th order mode) and of the two port waveguides. We adhere to the formulation and explicit expressions given in Ref. [38, 18]. Assuming that no reflections occur for the z-homogeneous region $0 < z < L$, one can write independent codirectional coupled mode equations for forward and backward propagating waves, and obtain independent reciprocal solutions in terms of transfer matrices that relate the amplitudes at both ends of the cavity segment.

Then combining the directional solutions for the waves in the cavity with the expressions for the guided wave reflection at the Bragg gratings allows to establish a CMT model for the full resonator device, analogously to the procedure described in Ref. [18] for the rectangular cavities with high-contrast facets. According to

Figures 4, 7, and 10 the CMT computations can adequately predict the power transfer characteristics of the present standing wave resonators. Up to a certain degree this justifies the assumptions made in Section 2.1.

Among the many approximations inherent in the CMT description is that the model restricts the coupling between the port waveguides and the cavity core to the homogeneous central cavity region (this region is of the same order of length as the Bragg gratings). Here one should observe that the interaction is dominated by waves with a specific effective mode index / mode angle in the bandgap interval of the Bragg reflectors; propagation of these waves is forbidden in the grating regions. This motivates neglecting the presence of the port waveguides for the modeling of the Bragg reflectors.

3 Numerical results

Besides the approximate CMT procedures, the devices were simulated by means of the mode expansion techniques as formulated in Refs. [31, 17]. The 2D-TE computations for the resonator devices use uniformly 100 expansion terms on a computational window $x \in [-20, 20]\,\mu$m that is confined by Dirichlet boundary conditions. All mode expansion results shown below correspond to these simulations. The wavelength spectra in Figures 4, 7, and Figure 10 are sampled with stepsizes of $0.2\,$nm ($\lambda \in [1.5, 1.6]\,\mu$m) and of $0.02\,$nm ($\lambda \in [1.548, 1.552]\,\mu$m).

We checked the results for a few representative sample configurations using a recently released commercial simulation tool [32], as well based on a bidirectional eigenmode propagation algorithm. In these computations the lateral computational window is enclosed by transparent boundary conditions (perfectly matched layers (PMLs)). At least in the 2D setting (cf. the appendix for a brief discussion of effects related to out-of-plane radiation in a 3D device), the structures under consideration generate only low levels of radiation; therefore we observed a reasonable agreement with the plotted results. Even with the reflecting Dirichlet boundary conditions at the borders of the $40\,\mu$m computational window (note the total device length of $203\,\mu$m), the mode expansion algorithm is apparently able to properly predict the guided power transmission. The small power fractions that correspond to the lateral radiation losses are transferred to the large set of nonguided basis fields, in contrast to the CMT approach, where the optical power remains confined to the few directional basis modes.

3.1 Symmetrical standing wave resonator

Figure 4 shows the spectral response for a device according to the specification of Section 2.1. The resonator is excited in port A by the right traveling guided mode of the lower core. For most wavelengths, most of the input power is directly transmitted to port B. Resonant states appear as a drop in P_B and a simultaneous increase of the reflected and dropped power fractions P_A, P_C, and P_D.
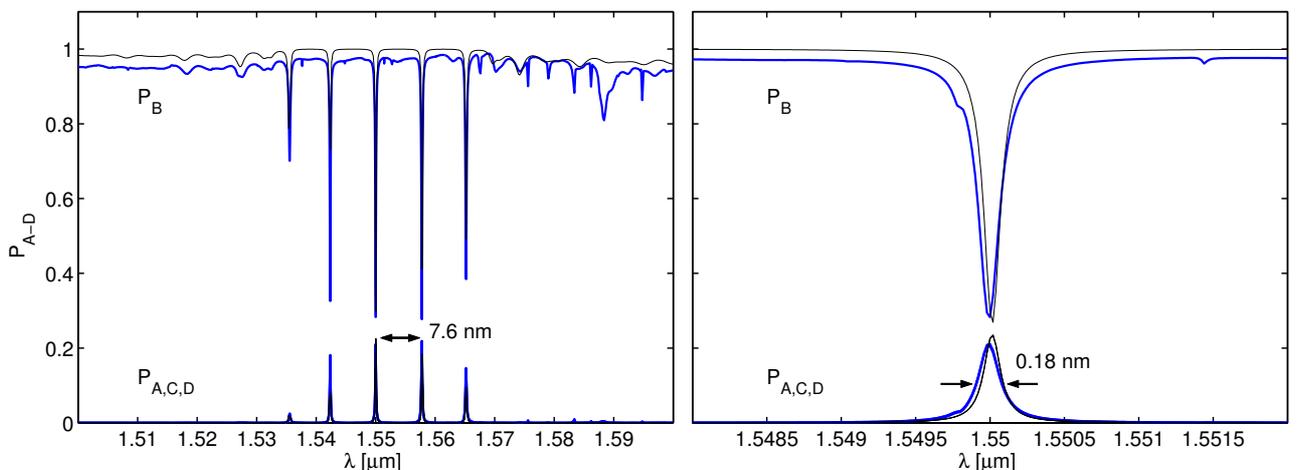

Figure 4: Spectral response of a resonator according to Figure 1 with the parameters of Table 1. P_A to P_D are the relative power fractions that are reflected or transmitted into ports A to D. The curves related to P_A, P_C, and P_D are almost completely superimposed. Bold lines correspond to the rigorous mode expansion computations, the thin lines indicate the CMT results.

As expected, the major resonances are restricted to the range of high reflectivity of the Bragg gratings (cf. Figure 3). The finesse of the resonator is 42, here defined as the ratio between the free spectral range and the width at half maximum.
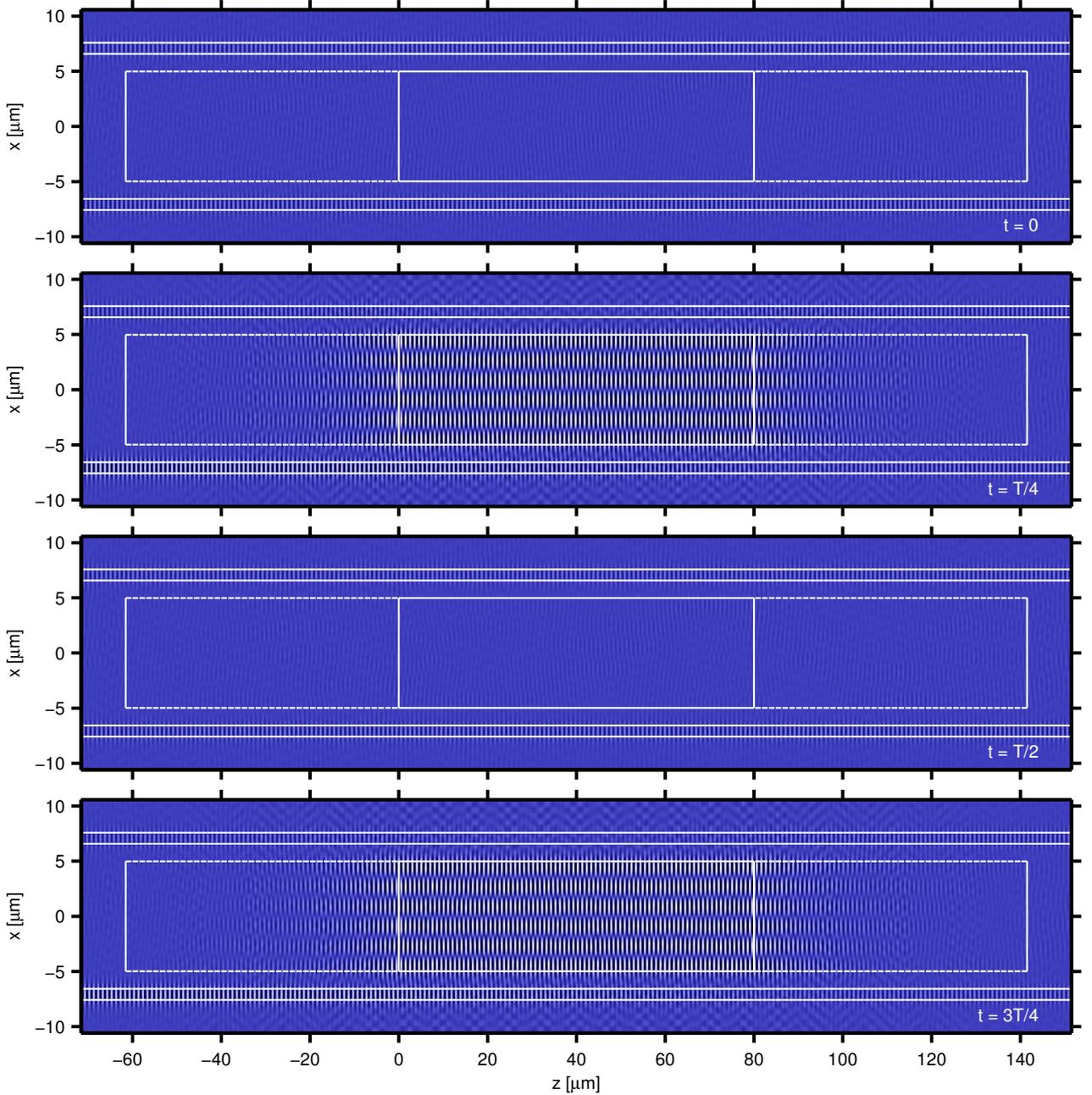

Figure 5: *Field pattern at resonance, for a grating assisted standing wave resonator according to the specification of Table 1, for $\lambda = 1.55\,\mu$m. The gray scale levels correspond to the physical electric field E_y, evaluated at four time positions that are equally distributed over one period $T = \lambda/c$. The dashed white horizontal lines indicate the regions of the Bragg gratings.*

Figure 5 illustrates the field pattern for the central resonance at the design wavelength $\lambda_0 = 1.55\,\mu$m. One finds outwards traveling waves in the waveguides corresponding to ports B, C and D. The superposition of the unit input and of the reflection with lower amplitude gives rise to a partly standing and partly traveling wave in port A. An almost purely standing wave is visible inside the cavity, with decaying amplitudes in the regions of the Bragg reflectors. Five horizontal nodal lines can be observed; hence it is indeed the 5-th order mode of the cavity that this resonance is built upon. The power transfer levels at this resonance are computed to be $P_A = P_C = P_D = 0.21$, and $P_B = 0.28$; these values are already close to the theoretical limit [16] of a balanced transmission of 25% of the input power into the four output ports.

3.2 Detuned Bragg reflectors

The variety of parameters in the device specification offers many possibilities for refinements or optimization. Accepting the rating of the device performance in terms of the finesse, one could try to enlarge that quantity virtually to infinity by trying to suppress all but the central resonance in the spectrum of Figure 4. The peaks are restricted to the wavelength interval that is defined by the high reflectivity region of the Bragg reflectors. Consequently a way to suppress the neighbouring resonances could be to use weaker Bragg gratings with a narrower bandgap region. An analogous effect should be achievable by increasing the spectral distance of the Fabry-Perot resonances via shortening the homogeneous part of the cavity and simultaneously decreasing the gap width to maintain a certain coupling strength. Both modifications would basically require to entirely redesign the resonator.
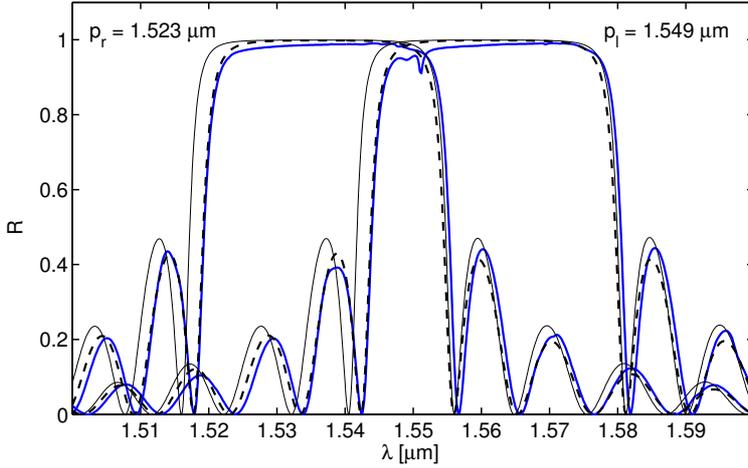

Figure 6: Reflectivity curves of Bragg reflectors according to Figure 2 and Table 1, with periods $p = 1.523\,\mu$m (continuous) and $p = 1.549\,\mu$m (dashed). The thin lines correspond to the plane wave model; bold lines indicate the results of rigorous mode expansion simulations (continuous) and of the CMT model (dashed).

As a third alternative, one can apply gratings with the same wide bandgap region as before, but with slightly altered period lengths, such that their bandgaps overlap in only a small interval around the target wavelength. Figure 6 gives an example for the present parameters. Here the gratings are based on the previous two different refractive index values, hence the reflectors can be defined by means of the same technological steps as the cavity and the port waveguides.
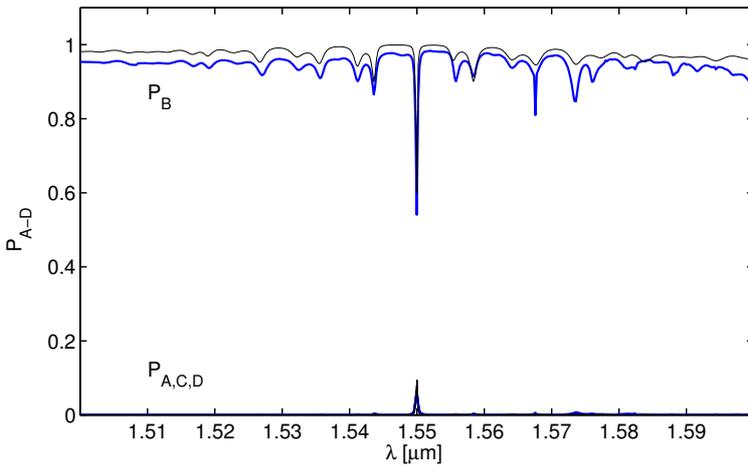

Figure 7: Spectral response of an asymmetrical resonator device with detuned, nonidentical Bragg reflectors; results of rigorous calculations (bold lines) and of the CMT model (thin curves). Parameters are as given in Table 1, with $L = 80.006\,\mu$m and with grating periods of $p = 1.523\,\mu$m and $p = 1.549\,\mu$m for the left and right reflector. (cf. Figure 6).

As expected, only a single resonance appears in the spectral response of a device where, when compared to the specification of Table 1, the left reflector has a slightly shorter period of $p = 1.523\,\mu$m, while the right Bragg grating is made with a longer period of $p = 1.549\,\mu$m. Figure 7 shows the results of the corresponding simulations. Along with the period length the complex reflection coefficients of the gratings at the target wavelength λ_0 change. Therefore, to reestablish the resonance at λ_0, the cavity length has to be slightly adjusted to a new value $L = 80.006\,\mu$m. Unfortunately the reflectivity curves of the waveguide Bragg gratings in the bandgap region exhibit a slightly tilted top, with the reflectivity at the short wavelength end of the bandgap being somewhat lower than at the long wavelength end (cf. e.g. Ref. [39]). The lower reflectivity leads to a

resonance that is less pronounced than for the configuration with identical Bragg reflectors with their bandgap centered around the target wavelength.

Only small modifications are necessary to detune the original configuration towards the single-resonance device, where the alterations in cavity length and in grating period could be replaced by a change of the relevant effective mode indices in the cavity and in the grating regions by electrooptical or thermooptical means. Perhaps this opens up a possibility for a dynamical adjustment of the resonator.

3.3 Add-drop filter

At resonance the present device distributes the input power almost equally among all four ports. This is not serviceable for an application as an add-drop filter, where one would prefer to have the resonant output directed to a single drop port. With conventional rectangular cavities, this functionality can be realized [16, 17] by placing two equal cavities between the port waveguides. Figure 8 sketches that concept when transferred to the present grating assisted Fabry-Perot resonators.
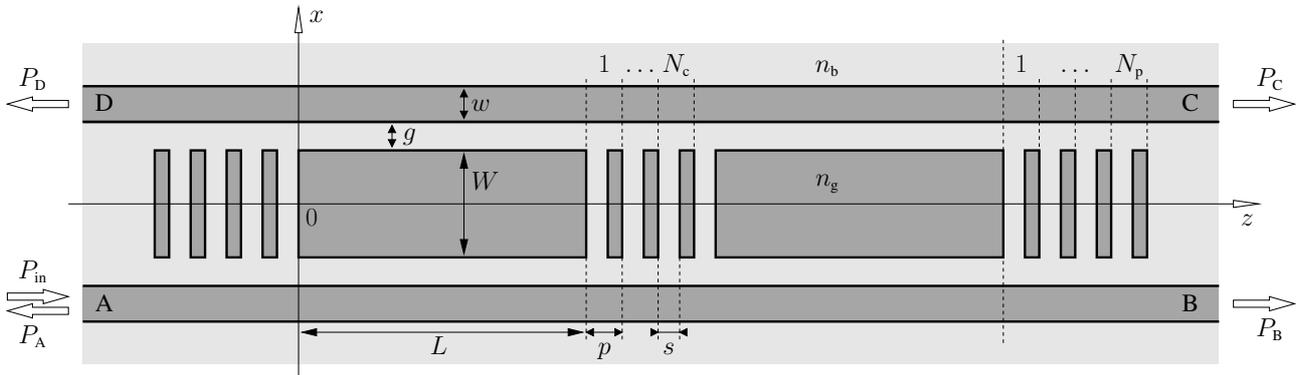

Figure 8: Add-drop filter, constituted by two cascaded rectangular cavities. Parameters are as introduced in Figure 1 and Table 1, with identical left and right Bragg reflectors, but with a shorter central reflector consisting of only N_c periods.

Compared to the single cavity configuration, only one new parameter is introduced, that specifies the distance between the individual cavities. According to theoretical considerations [16] and to numerical experiments [17], one can expect that besides the coupling via the port waveguides a certain level of direct interaction between the separate cavities is required to establish the desired type of resonance. Therefore we employ a central grating that is shorter than the original Bragg reflectors, such that the resonant field patterns of the individual cavities overlap. As illustrated by Figure 5, these field shapes decrease in envelope amplitude with growing distance from the homogeneous central segment. Hence, by adjusting the cavity separation, i.e. by changing the number of periods in the intermediate Bragg grating, one can control the strength of the direct coupling between the two cavities. Figure 9 shows how this change influences the power transfer characteristic of the composite device at the resonance wavelength.
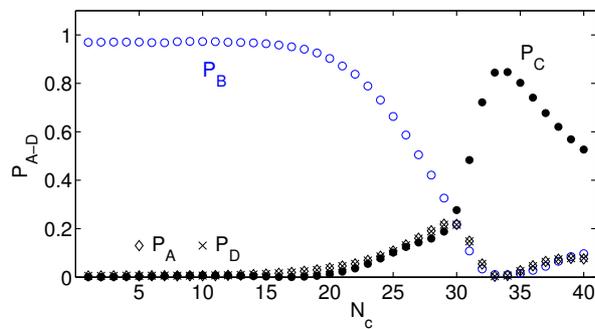

Figure 9: Power transmission through the filter device of Figure 8 versus the number N_c of periods in the central grating, for fixed input wavelength $\lambda = 1.55\,\mu$m.

Just as in the case of conventional rectangular resonators, where the interaction is caused by overlaps of evanescent field tails, here the overlaps of the decaying fields in the Bragg gratings effect an additional coupling of the individual cavities (on a much larger length scale than for the evanescent fields). For a small number of periods in the central grating, the device acts as a single cavity resonator that is off-resonance at the constant wavelength

prescribed in Figure 9. For $N_c = 30$ a resonance as found before is excited, with quarter transmission to all ports. The corresponding field pattern shows simultaneously appearing high intensities in both cavities. The extremal transfer characteristic is reached for $N_c = 33$, where only about 1% of the input power is reflected to ports A and C or transmitted to B, while a major part of the power is dropped in forward direction to port C. Here the resonant field pattern exhibits high intensities in both cavities as well, but now alternating in time: The standing wave in one of the cavities is at its maximum when the field in the other cavity assumes its zero level, and vice versa. These phenomena are entirely analogous to what has been observed for ordinary rectangular resonators [17].
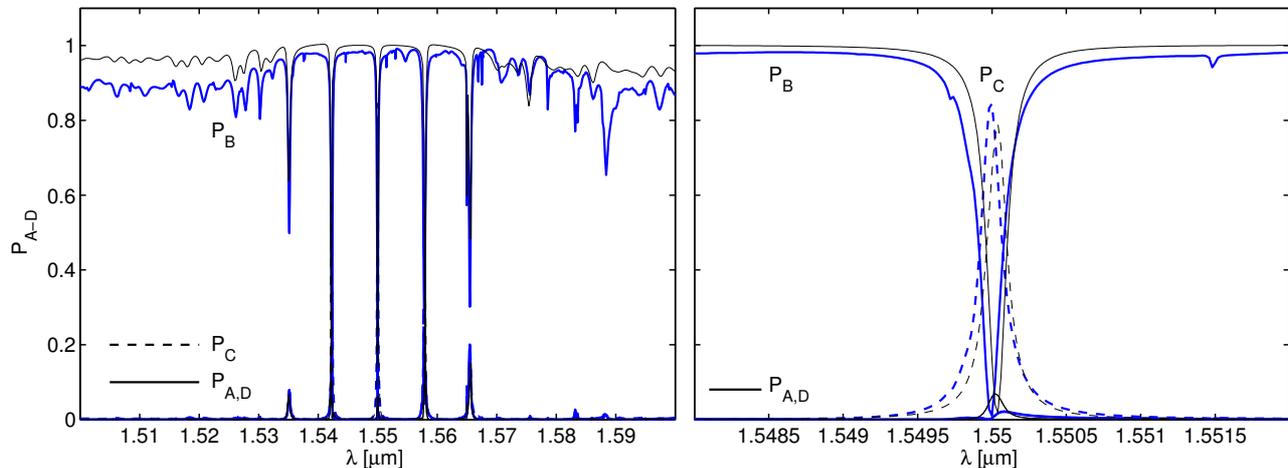

Figure 10: Spectral response of an add-drop filter device according to Figure 8 and Table 1, with $N_c = 33$ periods in the central reflector; the total length of the device is $334\,\mu m$. At the resonance $\lambda = 1.55\,\mu m$, the extremal relative levels of power transmission are $P_A = P_B = P_D = 0.01$, $P_C = 0.84$. The bold lines correspond to rigorous calculations; the thin curves were computed with the CMT model.

Besides the peak at $1.55\,\mu m$, the other resonances of the single cavity appear as well in the spectrum (Figure 10) of the composite device. While for the entire wavelength range the backward directed amounts of power P_A and P_D almost coincide, the strong deviation of the forward drop P_C from P_A and P_D remains restricted to the pronounced central resonance (around the neighboring peak at $\lambda = 1.542$, one observes extremal relative levels of $P_A = P_D = 0.20$, $P_B = 0.22$, $P_C = 0.34$). Further away from that wavelength region, the double cavity device exhibits the qualitative transmission characteristic of the single cavity resonator.

4   Concluding remarks

Based on quite simple design guidelines and moderate numerical means, the former results clearly demonstrate the working principle of the grating assisted rectangular microresonators, at least in terms of numerical simulations. We find the shape of resonances as predicted for high contrast standing wave resonators with finite waveguide segments as cavities, but in the present case with technologically more realistic refractive index contrasts, with an increased, but still reasonable length of the devices. Just as two conventional rectangular resonators, two Bragg grating based Fabry-Perot cavities can be cascaded such that at resonance the composite device directs the major part of the input power into a single drop port, as it is required for an add-drop filter application.

The (surprising) agreement between the quite approximative coupled mode theory model and the rigorous simulations justifies with hindsight the application of the design heuristics, that was based on the interaction between the confined modes of the port waveguides and merely one specific guided mode of the central cavity. This finding will be particularly relevant for any steps towards full three dimensional simulations, where the coupled mode model is the one that is most likely to be extendable to 3D within reasonable limits of computational effort.

The present design leaves plenty of room for further optimization. Apart from the theoretical limit of equal quarter transmission to all four ports at resonance, this concerns in particular the Bragg reflectors: Modifying

9

the grating with the aim of a narrow, properly positioned bandgap (probably at the cost of an increased device length) should allow to restrict the spectral response to a single resonance. We have demonstrated that this effect can be achieved alternatively by means of two slightly different Bragg gratings at both ends of the cavity, adjusted such that their regions of high reflectivity overlap in only a narrow wavelength region. This leads to devices with in principle infinite free spectral range and finesse. Perhaps a dynamic detuning could be considered: If made active (by electrooptically or thermooptically influencing either the cavity, i.e. by shifting the spectral position of the resonance, or by influencing the grating regions, such that the overlap of the bandgap regions can be adjusted), in its "on" state the device would drop a single wavelength, while otherwise all input wavelengths are directly transmitted.

Appendix

Assuming that the visualized device will be realized on the basis of embedded rectangular waveguide cores as sketched in Figure 11(a), the parameter values used above $n_g = 1.6$, $n_b = 1.45$ correspond to the effective index projection (top view) of the three dimensional structure, at the design wavelength of $\lambda_0 = 1.55\,\mu$m. Obviously, when viewed as an approximation of that 3D structure, the present model and the numerical results neglect entirely any effects related to light propagation in the vertical (y-) direction. Apart from polarization issues, in particular losses due to out-of-plane scattering in the grating regions are not accounted for.
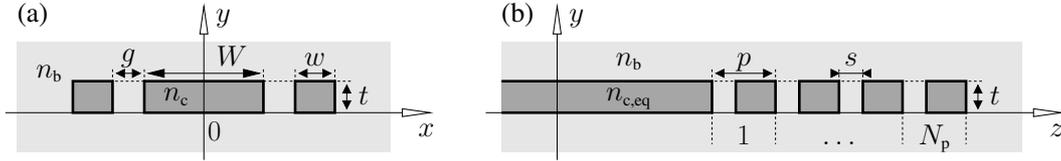

Figure 11: (a): Cross section of the hypothetical 3D device, rectangular Si_3N_4 cores (refractive index $n_c = 1.98$) surrounded by a SiO_2 background medium ($n_b = 1.45$), with a common channel thickness of $t = 0.223\,\mu$m. (b): Side view of the Bragg grating region of the envisioned 3D device. See the text for details on the choice of the equivalent core refractive index $n_{c,eq}$.

For a rough estimation of that effect we consider the Bragg gratings again, this time using a 2D restriction to the y-z-plane (side view). Figure 11(b) illustrates the configuration. The — admittedly quite heuristic — dimensionality reduction procedure has to take into account that a higher order mode of the cavity is relevant for the resonator operation. In the 3D device, this mode is characterized by a unique effective mode index, where the previous vertical projection led to the value of $n_{eff} = 1.540$. With the lateral projection being meant as an approximation of the same 3D structure, the guided mode of the cavity core can be expected to have the same effective mode index. We realized this constraint by replacing n_c by the lower value $n_{c,eq} = 1.853$. With this core refractive index, the single guided TE mode of the slab in Figure 11(b) propagates with the required effective mode index n_{eff} (Note that a core refractive index of n_c would correspond to a mode profile that is constant along x).
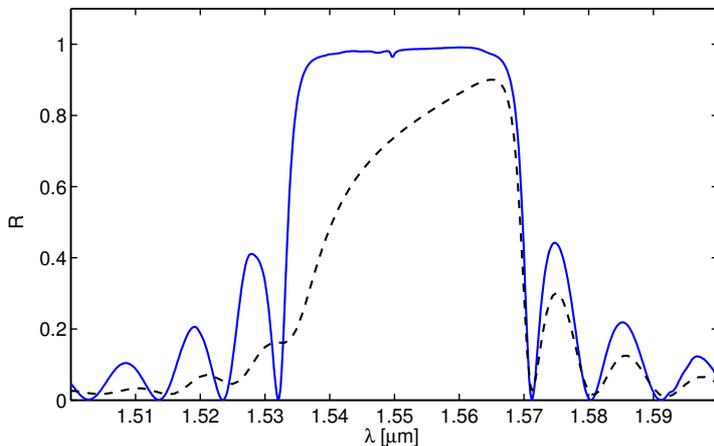

Figure 12: Reflectivity R of Bragg-reflectors according to the specifications of Figures 2, 11(b), and Table 1, versus the vacuum wavelength, for Bragg gratings with 40 periods. The continuous line corresponds to the reflectivity of the guided 5-th order mode in the "top view" approximation (data from Figure 3). The dashed curve indicates the reflectivity of the fundamental mode according to the "side view" projection.

10

This choice of the permittivity profile for the y-z model leads to a spectral reflectivity that preserves at least some features of the previous simulations. Figure 12 compares the results. Radiation losses are to be estimated, therefore the additional simulations were carried out with the commercial tool [32], using PML boundary conditions with the bidirectional eigenmode propagation algorithm.

The new viewpoint leads to a spectral characteristic that still exhibits a high reflectivity region at the position of the former bandgap, unfortunately now with a smaller maximum level and with a pronouncedly tilted top. The vertical losses predicted in this way are likely to degrade the performance of the 3D resonator, certainly at the position of the present target wavelength. Assuming that the curve can indeed be regarded as a realistic estimate of the loss levels that are to be expected for the approximated 3D structure, for the realization of the 3D device one would consequently have to redesign the Bragg gratings in three spatial dimensions. Apart from a slight reduction of the grating period in order to shift the high reflectivity region towards the target wavelength, starting points could be to switch to a different grating order (when counting bandgap regions in a plot of the reflectivity versus the grating period, the present parameters describe third order gratings), or to further reduce the refractive index contrast, at the cost of an increased grating length.

Acknowledgements

References

[1] R. A. Soref and B. E. Little. Proposed N-wavelength M-fiber WDM crossconnect switch using active microring resonators. *IEEE Photonics Technology Letters*, 10(8):1121–1123, 1998.

[2] S. T. Chu, B. E. Little, W. Pan, T. Kaneko, S. Sato, and Y. Kokubun. An eight-channel add-drop filter using vertically coupled microring resonators over a cross grid. *IEEE Photonics Technology Letters*, 11(6):691–693, 1999.

[3] B. E. Little, S. T. Chu, W. Pan, and Y. Kokubun. Microring resonator arrays for VLSI photonics. *IEEE Photonics Technology Letters*, 12(3):323–325, 2000.

[4] Next-generation active integrated optic subsystems. Information society technologies programme of the European Commission, project IST-2000-28018, http://www.mesaplus.utwente.nl/nais/.

[5] E. A. J. Marcatili. Bends in optical dielectric guides. *The Bell System Technical Journal*, September:2103–2132, 1969.

[6] D. R. Rowland and J. D. Love. Evanescent wave coupling of whispering gallery modes of a dielectric cylinder. *IEE Proceedings, Pt. J*, 140(3):177–188, 1993.

[7] B. E. Little, S. T. Chu, H. A. Haus, J. Foresi, and J.-P. Laine. Microring resonator channel dropping filters. *Journal of Lightwave Technology*, 15(6):998–1005, 1997.

[8] M. K. Chin and S. T. Ho. Design and modeling of waveguide-coupled single-mode microring resonators. *Journal of Lightwave Technology*, 16(8):1433–1446, 1997.

[9] F. C. Blom, H. Kelderman, H. J. W. M. Hoekstra, A. Driessen, Th. J. A. Popma, S. T. Chu, and B. E. Little. A single channel dropping filter based on a cylindrical microresonator. *Optics Communications*, 167:77–82, 1999.

[10] B. E. Little, J.-P. Laine, and H. A. Haus. Analytic theory of coupling from tapered fibers and half-blocks into microsphere resonators. *Journal of Lightwave Technology*, 17(4):704–715, 1999.

[11] S. V. Boriskina and A. I. Nosich. Radiation and absorption losses of the whispering-gallery-mode dielectric resonators excited by a dielectric waveguide. *IEEE Transactions on Microwave Theory and Techniques*, 47(2):224–231, 1999.

[12] D. J. W. Klunder, E. Krioukov, F. S. Tan, T. van der Veen, H. F. Bulthuis, G. Sengo, C. Otto, H. J. W. M. Hoekstra, and A. Driessen. Vertically and laterally waveguide-coupled cylindrical microresonators in Si_3N_4 on SiO_2 technology. *Applied Physics B*, 73:603–608, 2001.

[13] D. J. W. Klunder, M. L. M. Balistreri, F. C. Blom, H. J. W. M. Hoekstra, A. Driessen, L. Kuipers, and N. F. van Hulst. Detailed analysis of the intracavity phenomena inside a cylindrical microresonator. *Journal of Lightwave Technology*, 20(3):519–529, 2002.

[14] J. U. Nöckel and A. D. Stone. Ray and wave chaos in asymmetric resonant optical cavities. *Nature*, 385:45–47, 1997.

[15] E. Gornik. Geometrical shaping of microlaser emission patterns. *Science*, 280:1544–1545, 1998.

[16] C. Manolatou, M. J. Khan, S. Fan, P. R. Villeneuve, H. A. Haus, and J. D. Joannopoulos. Coupling of modes analysis of resonant channel add-drop filters. *IEEE Journal of Quantum Electronics*, 35(9):1322–1331, 1999.

[17] M. Lohmeyer. Mode expansion modeling of rectangular integrated optical microresonators. *Optical and Quantum Electronics*, 34(5):541–557, 2002.

[18] M. Hammer. Resonant coupling of dielectric optical waveguides via rectangular microcavities: The coupled guided mode perspective. *Optics communications*, 214(1–6):155–170, 2002.

[19] S. V. Boriskina, T. M. Benson, P. Sewell, and A. I. Nosich. Highly efficient design of spectrally engineered whispering-gallery-mode microlaser resonators. *Optical and Quantum Electronics*, 35(4/5):545–559, 2003.

[20] K. Djordjev, S.-J. Choi, S.-J. Choi, and P. D. Dapkus. Active semiconductor microdisk devices. *Journal of Lightwave Technology*, 20(1):105–113, 2002.

[21] K. Djordjev, S.-J. Choi, S.-J. Choi, and P. D. Dapkus. Vertically coupled InP microdisk switching devices with electroabsorptive active regions. *IEEE Photonics Technology Letters*, 14(8):1115–1117, 2002.

[22] S. T. Chu, W. Pan, S. Sato, T. Kaneko, B. E. Little, and Y. Kokubun. Wavelength trimming of a microring resonator filter by means of a UV sensitive polymer overlay. *IEEE Photonics Technology Letters*, 11(6):688–690, 1999.

[23] S. T. Chu, W. Pan, S. Suzuki, B. E. Little, S. Sato, and Y. Kokubun. Temperature insensitive vertically coupled microring resonator add/drop filters by means of a polymer overlay. *IEEE Photonics Technology Letters*, 11(9):1138–1140, 1999.

[24] S. Suzuki, Y. Hatakeyama, Y. Kokubun, and S. T. Chu. Precise control of wavelength channel spacing of microring resonator add-drop filter array. *Journal of Lightwave Technology*, 20(4):745–749, 2002.

[25] S. Follonier, M. Fierz, I. Biaggio, U. Meier, Ch. Bosshard, and P. Günter. Structural, optical, and electrical properties of the organic molecular crystal 4–N,N–dimethylamino–4'–N–methyl stilbazolium tosylate. *Journal of the Optical Society of America B*, 19:1990–1998, 2002.

[26] S. Kriswandhi. Simulation of a rectangular optical microresonator using bidirectional eigenmode propagation, 2002. C2V application note A2002005, Concept to Volume b.v. http://www.c2v.nl/software/support/appnotes/A2002005.pdf.

[27] M. Hammer and E. van Groesen. Total multimode reflection at facets of planar high contrast optical waveguides. *Journal of Lightwave Technology*, 20(8):1549–1555, 2002.

[28] M. Hammer and D. Yudistira. Grating assisted rectangular integrated optical microresonators. In J. Čtyroký, M. Hubalek, and F. Ondracek, editors, *Proceedings of the 11th European Conference on Integrated Optics ECIO'03, Vol. 1*, pages 357–360, Prague, 2003.

[29] C. Vassallo. *Optical Waveguide Concepts*. Elsevier, Amsterdam, 1991.

[30] G. Sztefka and H. P. Nolting. Bidirectional eigenmode propagation for large refractive index steps. *IEEE Photonics Technology Letters*, 5(5):554–557, 1993.

[31] M. Lohmeyer and R. Stoffer. Integrated optical cross strip polarizer concept. *Optical and Quantum Electronics*, 33(4/5):413–431, 2001.

[32] OlympIOs Integrated Optics Software. C2V, P.O. Box 318, 7500 AH Enschede, The Netherlands; http://www.c2v.nl/software/ .

[33] B. E. Little, S. T. Chu, W. Pan, D. Ripin, T. Kaneko, Y. Kokubun, and E. Ippen. Vertically coupled glass microring resonator channel dropping filters. *IEEE Photonics Technology Letters*, 11(2):215–217, 1999.

[34] M. Born and E. Wolf. *Principles of Optics, 7th edition*. Cambridge University Press, Cambridge, 1999.

[35] D. G. Hall and B. J. Thompson, editors. *Selected Papers on Coupled-Mode Theory in Guided-Wave Optics*, volume MS 84 of *SPIE Milestone Series*. SPIE Optical Engineering Press, Bellingham, Washington USA, 1993.

[36] J. H. Berends. *Integrated optical Bragg reflectors as narrow band wavelength filters*. University of Twente, Enschede, The Netherlands, 1997. Ph.D. Thesis.

[37] A. Yariv and P. Yeh. *Optical Waves in Crystals: Propagation and Control of Laser Radiation*. Wiley, New York, 1984.

[38] M. Lohmeyer, N. Bahlmann, O. Zhuromskyy, and P. Hertel. Radiatively coupled waveguide polarization splitter simulated by wave-matching based coupled mode theory. *Optical and Quantum Electronics*, 31:877–891, 1999.

[39] J. Čtyroký, S. Helfert, R. Pregla, P. Bienstmann, R. Baets, R. de Ridder, R. Stoffer, G. Klaase, J. Petráček, P. Lalanne, J.-P. Hugonin, and R. M. De La Rue. Bragg waveguide grating as a 1D photonic band gap structure: Cost 268 modelling task. *Optical and Quantum Electronics*, 34(5/6):455–470, 2002.